Journal of Materials Chemistry A

PAPER

View Article Online
View Journal | View Issue

Cite this: J. Mater. Chem. A, 2017, 5, 22662

A flexible all inorganic nanowire bilayer mesh as a high-performance lithium-ion battery anode†

Wei-Chung Chang, Tzu-Lun Kao, Yow Lin and Hsing-Yu Tuan *

Received 24th August 2017
Accepted 3rd October 2017

DOI: 10.1039/c7ta07472g

rsc.li/materials-a

Herein, we report a flexible, binder-free inorganic nanowire bilayer mesh as a lithium-ion battery anode that provides high practical areal, gravimetric, and volumetric capacities. The configuration of the binder-free inorganic nanowire bilayer mesh anode is solely composed of two layers of nanowire fabric with one layer of germanium (Ge) nanowires and the other of copper nanowires. This nanowire electrode exhibited a high specific capacity of 1153 mA h g^{-1} when cycled at 0.1C, good rate-capability (359 mA h g^{-1} at a charge current density of 20 A g^{-1}, 20C), and long-term cycling life of 1000 cycles and 1300 cycles when operated at 1C and 10C (discharge rate was fixed at 1C), respectively. The tightly tangled bilayer Ge/Cu nanowire mesh provides not only a strong structure to prevent the detachment of active materials, but also better electrical conduction because the two layers of nanowires penetrate each other instead of making a clear boundary. Moreover, the loading of Ge nanowires on a 1 cm^2 Cu nanowire mesh is tunable within a wide range from 0.5 to 6 mg, corresponding to high areal capacities from 0.5 to 6 mA h cm^{-2} and volumetric capacity from 217 to 539 mA h cm^{-3}, which is nearly twice as high as that of commercial graphite anodes with one side coating (255 mA h cm^{-3}) and 10 times higher than those of reported Ge flexible electrodes made with CNFs. A full-cell battery with a capacity of 60 mA h composed of a Ge/Cu fabric anode and $Li(Ni_{0.5}Co_{0.3}Mn_{0.2})O_2$ cathode was assembled to power up a power tool and LED arrays; this provided a proof-of-concept example to implement the nanowire mesh structure into a current battery system.

Introduction

With the rapid technological development, the demand of high-energy density lithium-ion batteries (LIBs) has increased for mobile applications such as in smartphones, tablets, notebooks, digital cameras, and electric vehicles as well as in large grid energy storage and stationary energy storage.[1] The emerging high-tech and novel applications require foldable and bendable batteries with high volumetric and gravimetric energy density that can adapt to any electronic device. To meet these requirements for LIBs, replacement of low-theoretical specific capacity materials and design of self-supported electrodes are the ideal strategies to accomplish flexible and high-energy density LIBs.[2]

High-theoretical specific capacity materials, including Si (3579 mA h g^{-1}), P (2596 mA h g^{-1}), Ge (1384 mA h g^{-1}), and Sn (994 mA h g^{-1}), for LIB anodes are potential alternatives to commercial graphite anodes (372 mA h g^{-1}); however, they suffer from dramatic volume changes (~300%) arising from insertion/extraction of lithium ions during the charge/discharge process; this ultimately causes pulverization of active materials and leads to short battery cycle life.[3] In recent studies, the volume expansion problems have been overcome by nanostructurization of high-capacity materials that can significantly improve the cycling stability.[4–13] In addition, *via* creating self-supported electrodes and reducing the use of inactive materials, such as binders, conductive agents, and current collectors, in the electrode, the energy density of high capacity materials of the LIBs can be increased.[14]

Germanium (Ge) is a promising candidate for self-supported LIB anodes owing to its excellent rate capability and ultra-long-term cyclability.[15–20] The outstanding battery performance of Ge could be attributed to its high electric conductivity (10 000 times higher than that of Si),[21] high lithium-ion diffusion coefficient (400 times higher than that of Si),[22] and good capability to accommodate large volume expansion.[23] Recently, germanium has been reported that could be flexible and self-supported anodes for high performance LIBs by the integration of germanium nanomaterials with carbon nanotubes (CNTs),[24,25] carbon nanofibers (CNFs)[26,27] or 3D graphene nanofoam.[28–30] However, these nanostructures with CNTs, CNFs, or graphene have several practical concerns to be resolved: (i) CNTs, CNFs, and graphene are too fluffy to form a dense electrode, lowering the volumetric energy density; (ii) it is difficult to control the loading mass of Ge on CNFs or

Department of Chemical Engineering, National Tsing Hua University, 101, Section 2, Kuang-Fu Road, Hsinchu, Taiwan 30013, Republic of China. E-mail: hytuan@che.nthu.edu.tw; Tel: +86-3-571-5131 ext. 42509

† Electronic supplementary information (ESI) available. See DOI: 10.1039/c7ta07472g

graphene by the electrospinning method, chemical reduction, or vapor deposition. Therefore, the optimal design of a self-supported electrode involves the formation of a dense structure and loading of large amount of high capacity materials with reduced weight of all inactive materials.

Herein, we report a binder-free nanowire bilayer mesh structure composed of Ge nanowires and copper nanowires without other conductive agents. The mass of the active materials can be easily tuned, and this mesh as a lithium-ion battery anode provides high areal, gravimetric, and volumetric capacities. The bilayer mesh shows excellent performance during comprehensive tests of electrodes. The critical advantages of this structure are as follows: the entanglement of the two layers of nanowires not only forms a compact structure, which prevents the detachment of the active material, but also promotes electrical conduction because the two layers of nanowires penetrate each other instead of making a clear boundary. As proof-of-concept, the pouch-type batteries assembled by the large area layered Ge/Cu nanowire mesh anode and commercial $Li(Ni_{0.5}Co_{0.3}Mn_{0.2})O_2$ cathode with an areal capacity of 3 mA h cm^{-2} can be applied in power tool and LED arrays.

Experimental

Materials

Diphenylgermane (DPG, 95%) was purchased from Gelest. Hydrogen tetrachloroaurate(III) trihydrate (99.99%), tetraoctylammonium bromide, (TOAB, 98%), sodium borohydride ($NaBH_4$, 98%), anhydrous toluene (99.99%), anhydrous benzene (99.8%), ethanol (99.8%), 1-dodecanethiol (98%), hydrofluoric acid (48 wt%), oleylamine (OLA, 70%), and diethyl carbonate (DEC) were purchased from Sigma-Aldrich. Copper chloride (CuCl, 99.99%) was purchased from Alfa. Fluoroethylene carbonate (FEC), electrolyte (1 M $LiPF_6$ in ethylene carbonate (EC) : dimethyl carbonate (DMC) 1 : 1 (v/v)), lithium hexafluorophosphate ($LiPF_6$), copper metal foil, lithium metal foil, celgard membrane, and coin-type cell CR2032 were purchased from shining energy. Commercial $Li(Ni_{0.5}Co_{0.3}Mn_{0.2})O_2$ electrodes were purchased from vista advance technology. A polytetrafluoroethylene (PTFE) mold was purchased from Kunchuan plastic. Pouch-type battery components were purchased from MTI Shenzhen Kejingtar Technology. LEDs and power tool were purchased from an electronic equipment and appliance store.

Synthesis of Ge nanowires

Ge nanowires were prepared by the method described by Yuan *et al.*[15] To enhance the yield of the Ge nanowires, the synthesis was modified by employing monophenylsilane (MPS), which was proposed by Lu *et al.*[31] At first, a 10 ml titanium reactor was placed in an argon-filled glovebox to ensure an oxygen-free atmosphere in the reactor, which was then sealed and brought out from the glovebox. Next, the reactant solution was prepared in the argon-filled glovebox by mixing 0.34 ml DPG, 1.02 ml gold nanoparticle dispersion, 0.24 ml MPS, and 9.56 ml anhydrous benzene. For the synthesis of Ge nanowires, the titanium reactor was heated to 420 °C, followed by pressurization until the system pressure reached 800 psi. Then, 5 ml of reactant solution was loaded into the stored loop and then delivered into the reactor at a flow rate of 0.55 ml min^{-1} for 10 minutes. After this, the loading and delivering of the remaining reactant solution were operated at the same flow rate and time. The titanium reactor was then cooled by water bath until it reached room temperature. The Ge nanowires were obtained from the reactor and washed by centrifugation (8000 rpm, 5 minutes) using toluene to remove the byproducts and Ge particles. The Ge nanowires were then placed in a 20 ml sample vial and stored in an argon-filled glovebox for further use.

Surface passivation of Ge nanowires

To reduce oxidation resistance and improve dispersibility in an organic solvent, Ge nanowires were passivated using the method described by Yuan *et al.*[15] At first, Ge nanowires were immersed in 10 wt% HF for 15 min and then properly rinsed with methanol. Next, the dried HF-treated Ge nanowires along with 15 ml 1-dodecanethiol were added to a 20 ml sample vial, which was then sealed by a rubber septum and connected to a Schlenk line. The vial was heated to and held at 80 °C under an argon atmosphere under continuous stirring for 12 hours. Then, the thiolated Ge nanowires were precipitated and washed by centrifugation using toluene and ethanol (1 : 1 v/v) to remove excess 1-dodecanethiol. After this, the thiolated Ge nanowires were put in a 20 ml sample vial and stored in a glovebox for further use.

Synthesis of copper nanowires

Crystalline copper nanowires were synthesized by a self-seeded process.[32] The synthesis of copper nanowires involved two materials: oleylamine (OLA) and copper chloride (CuCl). In a typical synthesis, 3 mmol CuCl and 30 ml OLA were added to a 50 ml three-necked flask in a glovebox. Subsequently, the flask was removed from the glovebox. One side neck was sealed with a thermocouple set for temperature detection; the middle neck of the flask was connected to the Schlenk line for oxygen removal, and the other neck was sealed with a rubber septum. Next, the three-necked flask was purged with continuous argon flow at 110 °C for 50 minutes to remove the residual oxygen and water. Then, the flask was further heated to and held at 250 °C under continuous stirring for 50 min. The copper nanowires were obtained from the three-necked flask and washed by centrifugation (rpm, minutes) using toluene. The copper nanowires were then put in a 20 ml sample vial and stored in a glovebox for further use.

Preparation of the bilayer Ge/Cu nanowire mesh electrode

Herein, two dispersions were prepared, which were Ge nanowires in toluene and copper nanowires in toluene. At first, the dispersion of copper nanowires was drop-casted into a PTFE mold. After toluene fully evaporated, the dispersion of Ge nanowires was drop-casted onto the copper nanowires in the PTFE mold. When toluene fully evaporated, the bilayer Ge/Cu

nanowire electrode was removed from the mold and then annealed at 500 °C under a 5% H_2/95% Ar atmosphere for 90 minutes in a furnace to remove the surfactant and reduce the oxide layer on the copper nanowires surface. After annealing, the bilayer Ge/Cu nanowire electrode was stored in a glovebox for further assembly of lithium batteries. The mass loading of Ge nanowires was from 0.5 mg cm^{-2} to 6 mg cm^{-2} on the copper nanowires substrates, and it could be controlled by the concentration of the dispersion (Ge nanowires in toluene).

Characterization

SEM images were obtained using a field-emission scanning electron microscope (HITACHI, SU8010), operated at 15 kV accelerating voltage. The SEM samples were prepared by drop-casting toluene dispersion onto silicon wafers or copper plates and proper drying. The SEM images of the bilayer Ge/Cu nanowire electrode were obtained by adhering the electrode onto the silicon wafers or copper plates by carbon conductive tape. TEM images were obtained using the HITACHI H-7100 transmission electron microscope. The TEM samples were prepared by drop-casting toluene dispersion onto 200 mesh carbon-coated copper grids.

Lithium-ion battery assembly and electrochemical characterization

Coin-type half-cells. Typically, the active material mass loading of the bilayer Ge/Cu nanowire electrode was from 0.5 to 0.8 mg cm^{-2}; moreover, the electrochemical performance using high active material mass loading (from 3 mg cm^{-2} to 6 mg cm^{-2}) was evaluated. The coin-type half cells (CR2032) were prepared in an argon-filled glovebox. The coin-type half cells contained a bilayer Ge/Cu nanowire electrode (without a copper foil), lithium metal, and a separator wetted by an electrolyte, which contained 1 M $LiPF_6$ in diethyl carbonate/fluoroethylene carbonate (DEC/FEC) (7 : 3 v/v). Charge/discharge cyclic performance of the layered Ge/Cu nanowire electrode was tested between 0.01 V and 1.5 V using Maccor Series 4000.

Pouch-type batteries. For a pouch-type battery assembly, the commercial $Li(Ni_{0.5}Co_{0.3}Mn_{0.2})O_2$ electrode connected to the positive terminal (aluminum tab) was used as a cathode, and the bilayer Ge/Cu nanowire electrode connected to the negative terminal (nickel tab) was used as an anode. In addition, a thin bar copper foil was put under the bilayer Ge/Cu nanowire electrode for connecting the electrode to the nickel tab. The cathode, anode, and separator were fixed at the aluminum-

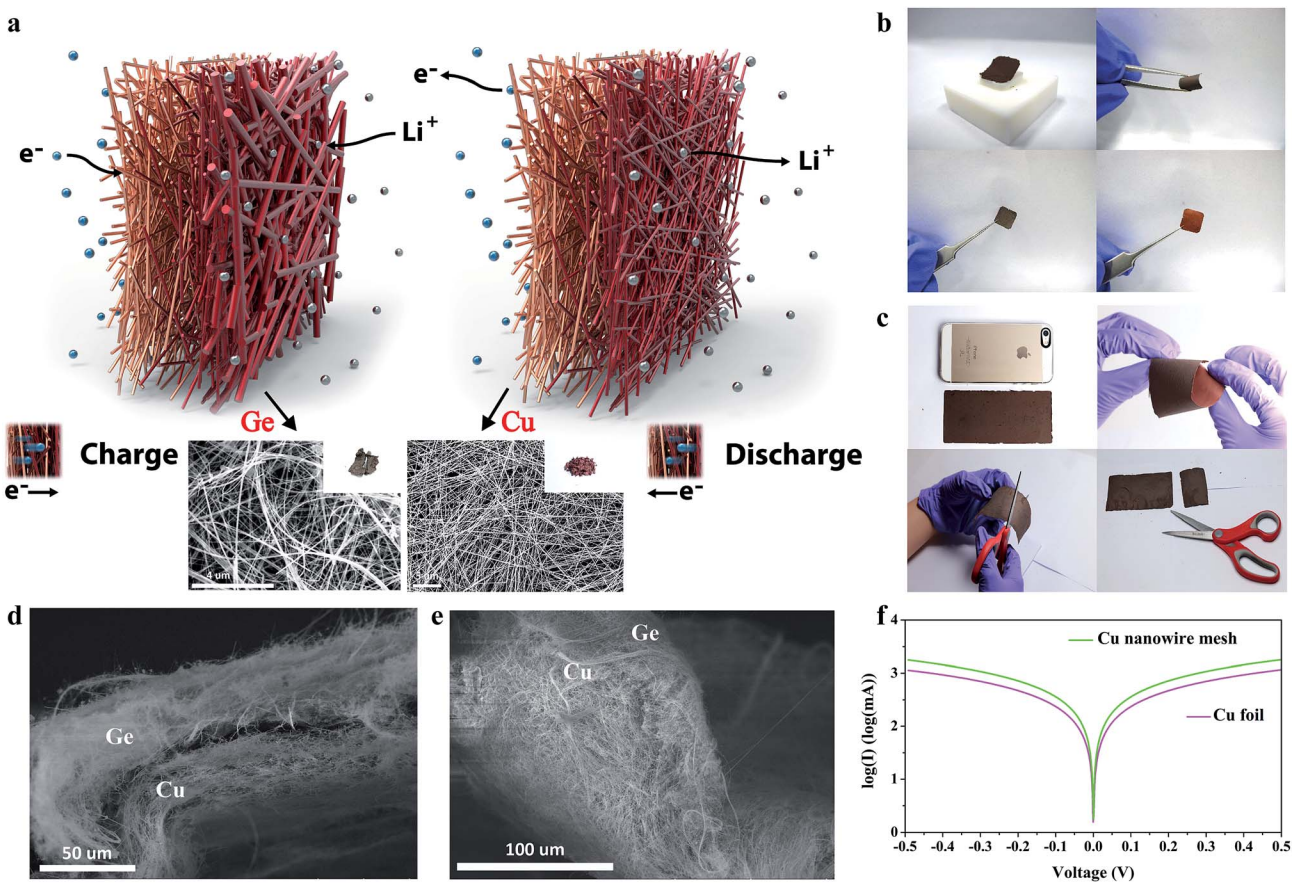

Fig. 1 Fabrication and characterization of the bilayer Ge/Cu nanowire mesh electrodes. (a) Schematic of the two-layer nanowire mesh electrode using copper nanowires as a substrate and Ge nanowires as an active material. (b) Images of the 1 cm × 1 cm bilayer Ge/Cu nanowire mesh electrode. (c) Images of a large area (5.2 cm × 12 cm) of the bilayer Ge/Cu nanowire mesh electrode, which can be easily trimmed by a utility knife. (d and e) Cross-section SEM images of a bilayer Ge/Cu nanowire mesh electrode, showing an intertwined structure at its interface. (f) Current–voltage characteristic of the copper nanowire mesh and copper foil.

laminated film, followed by the injection of the electrolyte into the aluminum-laminated film, which was then sealed by a compact heating sealer in a glovebox. The charge/discharge cyclic performances of pouch-type batteries were tested between 2.5 V and 4.2 V using Maccor Series 4000.

Result and discussion

Fabrication of the Ge/Cu bilayered mesh

Fig. 1a shows the schematic and working principles of a bilayer Ge/copper nanowire mesh electrode. Ge nanowires with an average diameter of 70 ± 20 nm and lengths over 100 μm were synthesized *via* the gold-seeded supercritical-fluid liquid solid (SFLS) growth method. Detailed analysis results, including scanning electron microscopy (SEM) images, transmission electron microscopy (TEM) images, EDS spectra, and electrical properties, of Ge nanowires are shown in Fig. S1.† Copper nanowires with an average diameter of 50 ± 15 nm and lengths over 20 μm were produced *via* the self-seeded process in oleylamine.[32] Bilayer Ge/Cu nanowire mesh electrodes were made by several steps (Fig. S2†). The dispersion of copper nanowires in toluene was drop-casted into a PTFE mold, and Cu nanowires automatically weaved themselves into the fabric during precipitation. As for the Ge nanowires layer, the dispersion of Ge nanowires in toluene was drop-casted onto the fully dried copper nanowires in a PTFE mold, and a bilayer Ge/Cu nanowire mesh formed after toluene fully evaporated. Once the Ge/Cu mesh electrode was removed from the PTFE mold, it was annealed at 500 °C under an argon/hydrogen atmosphere for two hours; this led to improved electrical conductivity of the mesh due to the removal of the organic residue and oxide layer on the surface of nanowires. Fig. 1b shows the images of the bilayer Ge/Cu nanowire mesh removed from a 1 cm × 1 cm PTFE mold, and the image of a 5.2 cm × 12 cm bilayer Ge/Cu nanowire mesh made with an upsized mold by the same process is shown in Fig. 1c. This large-sized bilayer Ge/Cu nanowire electrode can be easily tailored by shear into any shape suitable for later assembly of LIBs. Fig. 1d and e show the cross-section SEM images of a bilayer Ge/Cu nanowire mesh. It can be easily observed that the two layers of nanowires are partially intertwined together at the interface and create strong wire-to-wire adhesion, leading to a tightly tangled bilayer Ge/Cu nanowire mesh that prevents the detachment of the active material and provides better electrical conduction as the two layers of nanowires penetrate each other instead of making a clear boundary. The copper nanowire mesh was not pressed by a rolling machine; however, its conductivity was as well as that of the dense copper foil, as shown in Fig. 1f. Moreover, the areal mass of the copper nanowire mesh was in the proximity of 1.5 mg cm^{-2}, which was significantly lower than 8.7 mg cm^{-2} of copper foil with a 10 μm thickness (see Fig. S3†).

Electrochemical performance

The Ge/Cu bilayer nanowire mesh electrodes loaded with 0.5 mg Ge nanowires exhibit impressive cycling performance, as shown in Fig. 2. The columbic efficiency was 81% in the first cycle and

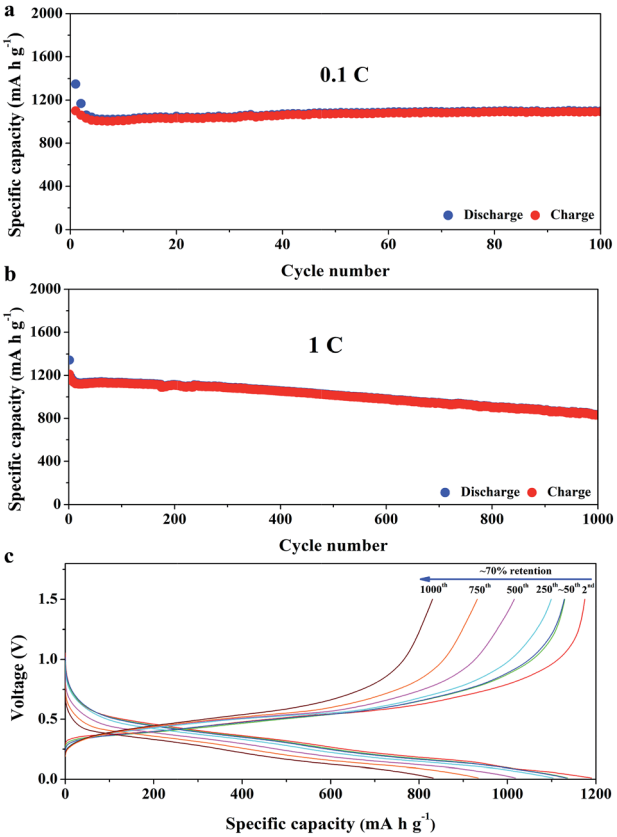

Fig. 2 Electrochemical performance of bilayer Ge/Cu nanowire mesh electrodes with the FEC/DEC electrolyte. (a) Cycling performance of the bilayer Ge/Cu nanowire mesh electrode at a rate of 0.1C between 0.1 V and 1.5 V. (b) Cycling performance obtained *via* a 1000-cycle test of the bilayer Ge/Cu nanowire mesh electrode at a rate of 1C (1st cycle at a rate of 0.1C). (c) Voltage profile of the bilayer Ge/Cu nanowire mesh electrode at a rate of 1C through 1000 cycles corresponding to (b).

remained at around 99% in the following cycles (Fig. S4†). The charge capacity retention with regard to the 5th cycle was over 99% after 100 cycles at a rate of 0.1C (100th cycle 1092 mA h g^{-1}), and the retention still maintained a fine value (over 70%) throughout 1000 cycles at a higher rate of 1C (1000th cycle 830 mA h g^{-1}). Additionally, the cycling performance of the Ge nanowire/Cu foil electrode was evaluated, as shown in Fig. S5.† The surface of copper is too smooth to adhere to the Ge nanowire mesh; this leads to the increase in contact resistance between the interface of Ge nanowire and Cu foil; as a result of this, rapid capacity fade occurs after several cycles. The capabilities of the bilayer Ge/Cu nanowire mesh electrodes to endure high discharge/charge current density cycling were evaluated, as shown in Fig. 3a and b, which revealed that bilayer Ge/Cu nanowire mesh electrodes could be operated at various current densities. The obtained charge capacities were 1153 mA h g^{-1} (0.1C, 0.1 A g^{-1}), 1120 mA h g^{-1} (0.5C, 0.5 A g^{-1}), 1081 mA h g^{-1} (1C, 1 A g^{-1}), 1028 mA h g^{-1} (2C, 2 A g^{-1}), 957 mA h g^{-1} (3C, 3 A g^{-1}), 924 mA h g^{-1} (4C, 4 A g^{-1}), and 855 mA h g^{-1} (5C, 5 A g^{-1}). Even at higher operational discharge/charge current densities of 10 A g^{-1} (10C), 15 A g^{-1}

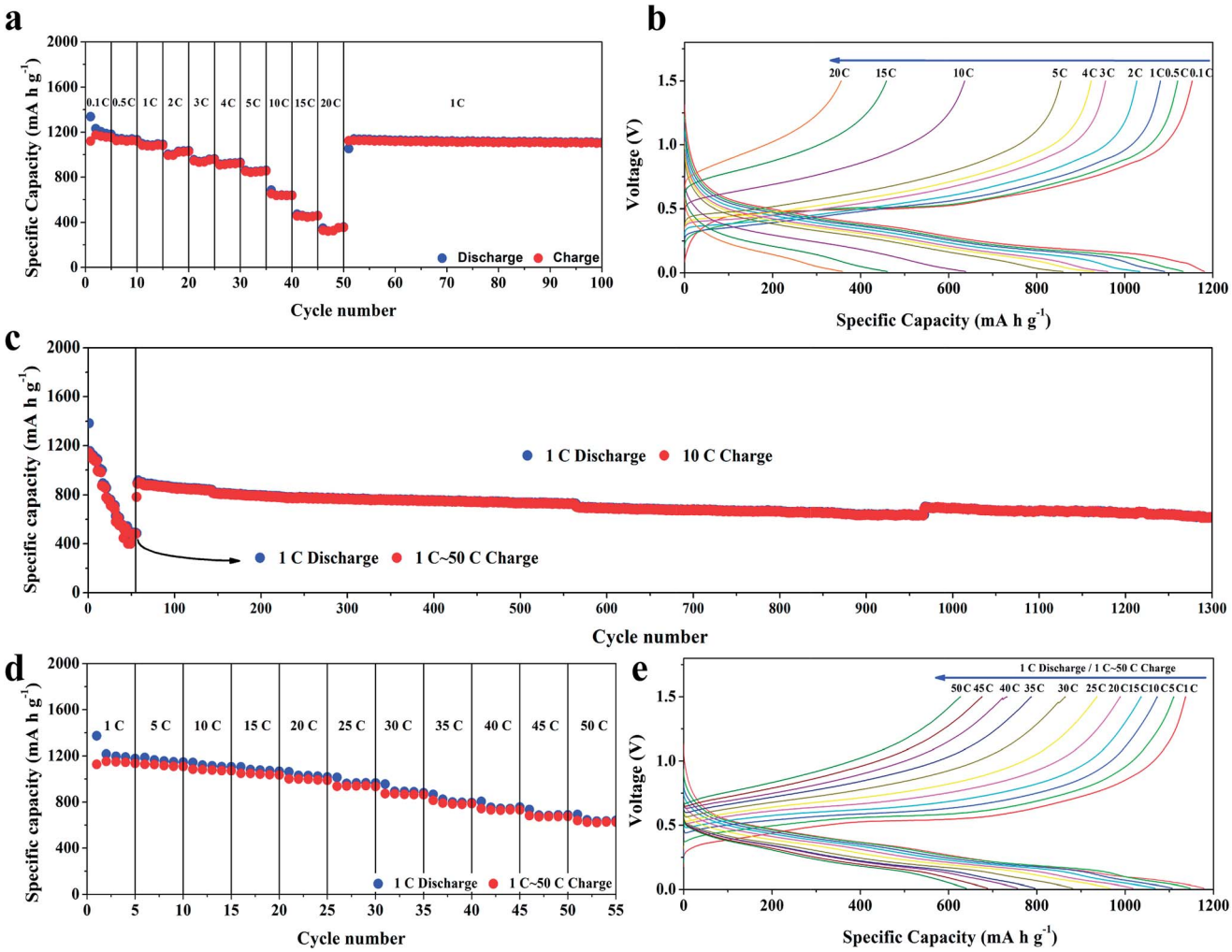

Fig. 3 Cycling performance of bilayer Ge/Cu nanowire mesh electrodes with the FEC/DEC electrolyte under various testing conditions. (a) The rate performance of the bilayer Ge/Cu nanowire mesh electrode at various rates from 0.1C to 20C for the initial 50 cycles followed by a rate of 1C for next 50 cycles. (b) Voltage profile of the bilayer Ge/Cu nanowire mesh electrode at various rates from 0.1C to 20C corresponding to (a). (c) The charge rate performance of the bilayer Ge/Cu nanowire mesh electrode discharge at a rate of 1C and charge at various rates from 1C to 50C for the initial 55 cycles followed by a discharge rate of 1C and a charge rate of 10C till 1300th cycle (1st cycle at a rate of 0.1C). (d) The charge rate performance of the bilayer Ge/Cu nanowire mesh electrode discharge at a rate of 1C and charged at various rates from 1C to 50C (1st cycle at a rate of 0.1C). (e) Voltage profile of the Ge/Cu nanowire mesh electrode at various charge rates from 1C to 50C corresponding (d). The data of (d and e) were different from those obtained during the initial 55 cycles, as shown in (c).

(15C), and 20 A g^{-1} (20C), the bilayer Ge/Cu nanowire mesh electrodes still retained a specific capacity of 639 mA h g^{-1}, 461 mA h g^{-1}, and 359 mA h g^{-1}, respectively. To simulate the utilization of energy storage device at various rates in real life, the bilayer Ge/Cu nanowire mesh electrodes were charged at various current densities from 1C (1 A g^{-1}) to 50C (50 A g^{-1}) but discharged at 1C, as shown in Fig. 3d and e. Evidently, the bilayer Ge/Cu nanowire mesh electrode has a surpassingly ultrafast discharging rate capability despite the fact that there are no any additional additives, which are crucial ingredients in conventional LIB design to promote the electrical conduction or prevent the electrode structure from collapsing, employed. As a result, a high discharge capacity of 1001 mA h g^{-1} was achieved at the charge current density of 20 A g^{-1} (20C). When the charge rate was elevated dramatically to 50C (50 A g^{-1}), the Ge/Cu electrode showed a charge capacity of 627 mA h g^{-1}, which was approximately twice the value of the theoretical capacity of graphite. As the charge rate was adjusted back to 10C afterwards, the bilayer Ge/Cu nanowire mesh electrode showed good resiliency with a charge capacity of 890 mA h g^{-1} and exhibited extraordinary long cycle life up to 1300 cycles (Fig. 3c).

The role of electrolytes and current collector in nanowire battery performance

To further confirm the improvements of the cycling stability and high-rate capability indeed attributed to the bilayer Ge/Cu nanowire mesh structure, the coin cells were disassembled. The Ge/Cu nanowire mesh electrode was obtained for subsequent analysis, as shown in Fig. 4a and b. After 200 cycles at a rate of 1C, the bilayer Ge/Cu nanowire electrode still exhibited

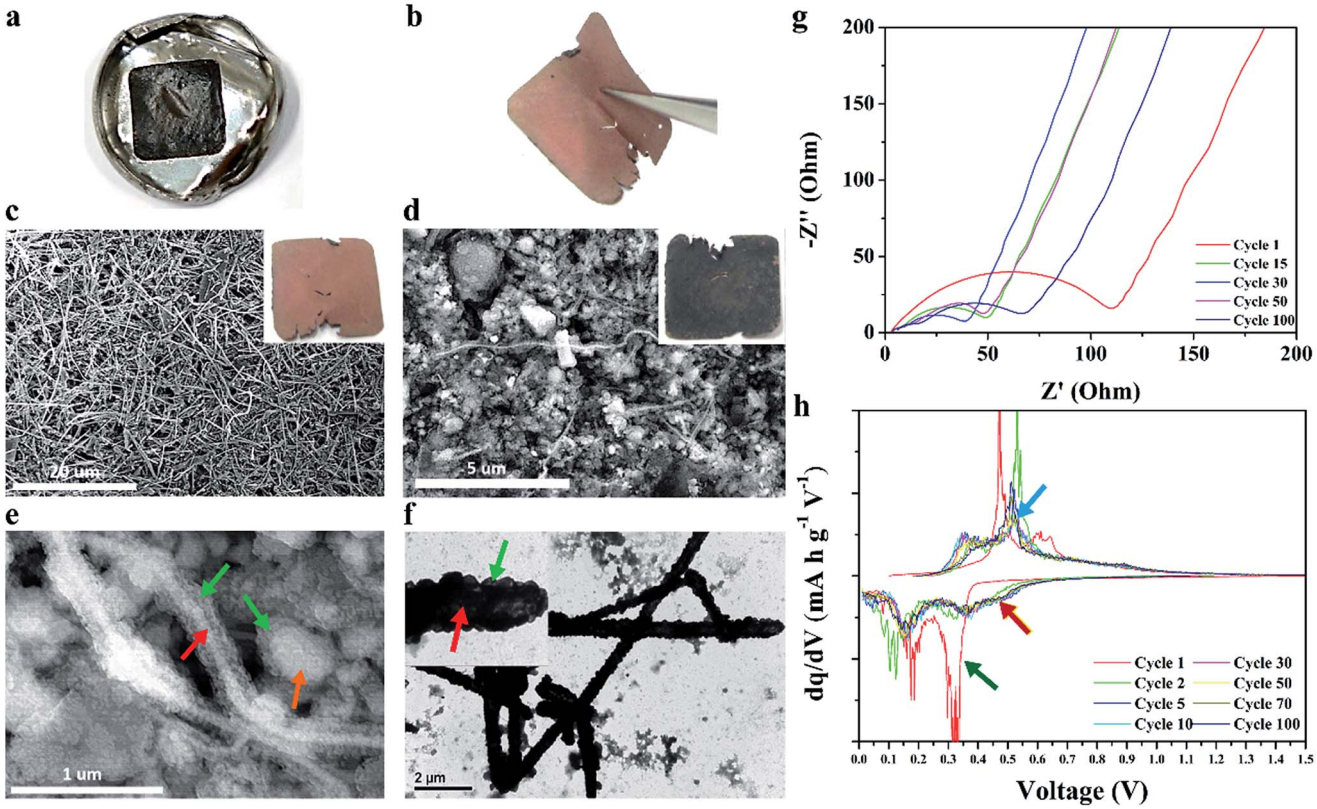

Fig. 4 Analysis of the bilayer Ge/Cu nanowire mesh electrode after 200 cycles at a rate of 1C with the FEC/DEC electrolyte. (a) Image of the disassembled CR2032 coin cell. (b) Image of the bilayer Ge/Cu nanowire mesh electrode, showing that the bilayer Ge/Cu nanowire mesh electrode peeled from the coin cell was still flexible and resilient. (c) The SEM image of the Cu layer of bilayer Ge/Cu nanowire mesh electrode. The inset shows the image of the Cu layer. (d) SEM image of the Ge layer of the bilayer Ge/Cu nanowire mesh electrode. The inset shows the image of the Ge layer. (e) High-magnification SEM image of Ge nanowires with the red arrow pointing out the Ge nanowire, the green arrows pointing out the SEI layers, and the orange arrow pointing out the pulverizing Ge particle. (f) TEM image of Ge nanowires with the red arrow and green arrow pointing out the Ge nanowire and compact SEI layer, respectively. (g) Nyquist plots of the bilayer Ge/Cu nanowire mesh electrode half-cell after various cycles: 1st, 15th, 30th, 50th, and 100th at a rate of 1C (1st cycle at a rate of 0.1C). (h) Differential capacity profile of the bilayer Ge/Cu nanowire mesh electrode with the initial cycle at a rate of 0.1C and the remaining 99 cycles at a rate of 1C. The green arrow points out the first cycle. The red and blue arrows point out that no obvious change occurred in the following 99 cycles.

flexibility; moreover, there was no flaking of the Ge nanowires (Fig. 4b). Furthermore, scanning electron microscopy (SEM) was used to observe the surface morphology of the bilayer Ge/Cu nanowire mesh electrodes, as shown in Fig. 4c and d, which disclosed information about the structural status of electrodes. Owing to the inert nature of copper nanowires with regard to electrochemical cycling in LIBs, the morphology of copper nanowires remained intact, and they still intertwined with the Ge nanowires, which were mostly fragmented. Use of a bit of copper nanowires as a supporting substrate plays a quite important role as copper nanowires can compactly contact the fragmented Ge nanowires and hold the electrode together without severe crashing; this provides a low resistance pathway for transferring electrons. In addition, the FEC-added electrolyte is another crux of the improvements. The growth of the solid electrolyte interface (SEI) on the surface of active materials is a well-known phenomenon that occurs during cycling; however, the brittle SEI may break because of expansion and contraction of the active materials during cycling, and the fresh surface of active materials is later re-exposed to the electrolyte; this leads to the re-formation of SEI, bringing about thicker SEI in each cycle.[4] Use of FEC as an additive is a common method to address this issue for high capacity materials.[18,33–37] During the FEC reduction (formation of the SEI film), it first transforms into VC followed by polymerization of VC to form the polycarbonate species. It is believed that polycarbonate can form tough SEI layers to accommodate the expansion and contraction;[38–41] thus, the FEC-added electrolyte system leads to a stabilized SEI film, decreasing the impedance for the processes of lithiation/delithiation as compared to the FEC-free electrolyte system.[38,42,43] As shown in Fig. 4e and f, compared to the EC-added electrolyte (Fig. S6 and S7†), the FEC-added electrolyte results in thinner and compact SEI layers on the surface of germanium nanowires, providing shorter path for the diffusion of lithium ions and improving the cycling performance. In addition to observing the morphology, the electrochemical behavior of the Ge/Cu nanowire mesh electrode was investigated *via* electrochemical impedance spectroscopy (EIS) and differential capacity profile plots obtained from different cycles, as shown in Fig. 4g and h. Except for the plot of the first

cycle, which corresponds to the lithiation of crystalline Ge and the formation of SEI, being different from other cycles,[44] no obvious changes have been observed in the Nyquist plots in the following cycles and the capacity profile plots after 100 cycles at a rate of 1C; this indicates a slow increase of resistance and the thickness of SEI during cycling.

Areal capacity

Based on the result of the anode performance, while the mass loading of Ge is increased to 3 mg cm^{-2}, the areal capacity can approximately achieve a value of 3 mA h cm^{-2}, which is sufficient for pairing with the commercial cathodes. We prepared the bilayer Ge/Cu nanowire mesh electrode with about 3 mg cm^{-2} Ge loading and tested it at a rate of 0.5C (1.5 mA cm^{-2}) as shown in Fig. 5a. The bilayer Ge/Cu nanowire mesh electrode was able to maintain an areal capacity of 2.93 mA h cm^{-2} through 50 cycles even when the mass loading of Ge was increased to 3 mg cm^{-2}. We also conducted an experiment with extreme mass loading of Ge in the Ge/Cu nanowire mesh electrode to investigate the limits of areal capacity, which was over twice as high as that of the commercial electrode. Despite obtaining a high areal capacity of 7.76 mA h cm^{-2} in the first cycle with the Ge mass loading of 5.88 mg cm^{-2}, the areal capacity quickly dropped to 4.13 mA h cm^{-2} after 50 cycles; this was probably due to the longer lithium-ion diffusion distance in the thick Ge nanowire layer.

Gravimetric capacity and volumetric capacity based on the total mass and the total volume of electrode

The total mass of the electrode is significantly reduced since the mass of Cu nanowire is only 1.5 mg – only one-sixth of 10 μm thick Cu foil. Moreover, only 3 mg of Ge is required to provide a current output of 3 mA h, whereas 10 mg traditional graphite is needed to deliver the same current output. The specific capacities against the cycle number based on the total mass of the electrode were re-plotted (Fig. 5b and d), which showed that Ge/Cu nanowire mesh electrode possessed better specific capacity and high rate-capability than commercial graphite and recent Ge or Si nanostructure (Tables S1 and S2†) on the basis of the total mass of the electrode. Even at a low areal mass loading of Ge (0.5 mg cm^{-2}), the bilayer Ge/Cu nanowire mesh electrode displayed higher specific capacity than the abovementioned cases. At high areal mass loadings of 3.07 mg cm^{-2} and 5.88 mg cm^{-2}, the respective reversible specific capacities of 706 and 863 mA h g^{-1} after 10 cycles are approximately 4 times higher than those of commercial graphite and outdistance those of previous Ge/Cu foil[8,15,18,45–57] and Si/Cu foil[43,58–67] reported in literature. As shown in Fig. 6 and Table S3,† we calculated the approximate electrode mass, volume, and the volumetric capacity on the basis of 100 mA h full cell with a graphite/Cu foil, Ge/Cu mesh, and other flexible Ge electrodes[26,27] as the anodes. The mass of graphite needed (0.29 g) for a one-sided-coated electrode having an areal capacity of 4 mA h cm^{-2} was

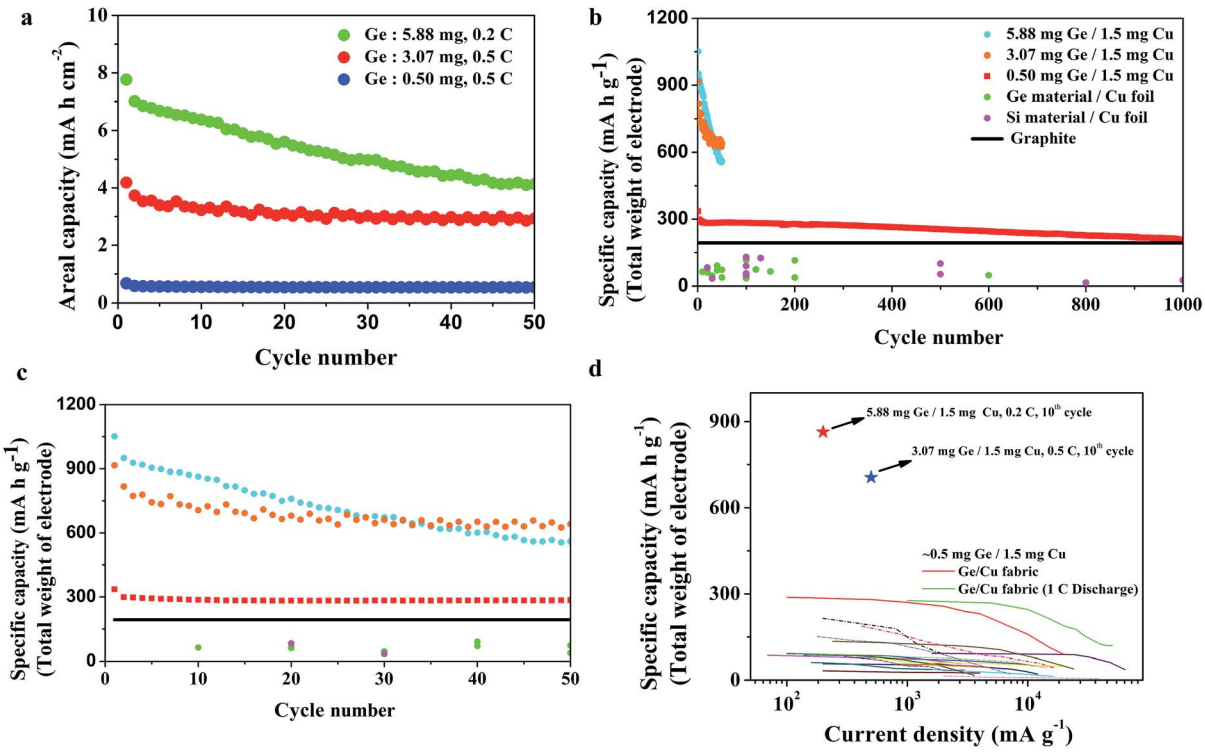

Fig. 5 Half-cell test at high loadings of active materials and graphic explanation of the bilayer Ge/Cu nanowire mesh electrode's superiority. (a) Cycling performance of the bilayer Ge/Cu nanowire mesh electrode with different active material loadings per unit area. (b) Specific capacity comparisons of the bilayer Ge/Cu nanowire mesh electrode, commercial graphite, and previous Ge, Si literatures obtained *via* calculating the total mass of the entire electrode, including active materials, binder, conductive agents, and current collector. (c) The initial 50 cycles, as shown in (b). (d) Rate-performance of the bilayer Ge/Cu nanowire mesh electrode and reported Ge and Si literatures.

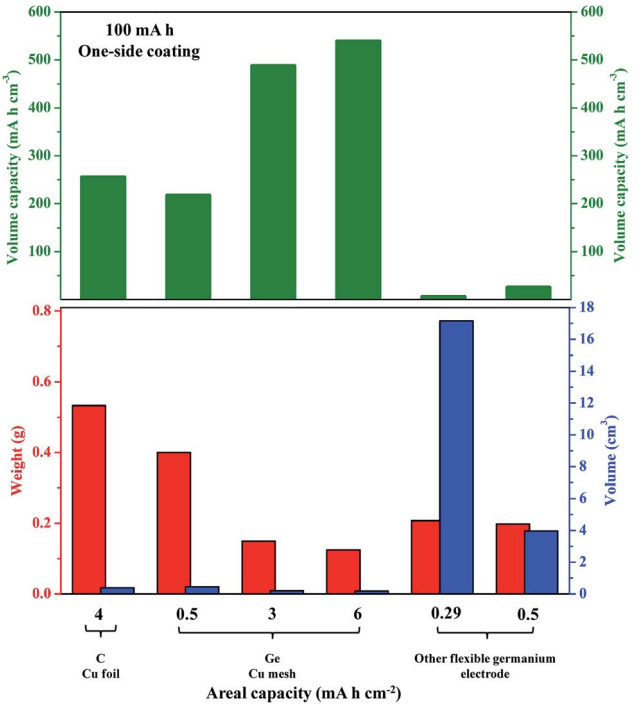

Fig. 6 Volumetric capacities theoretically calculated from the areal capacity and the total volume of the electrode, where the mass of the active material required for providing certain areal capacity is theoretically calculated based on the specific capacities normally exhibited by graphite (330 mA h g^{-1}) and Ge (1000 mA h g^{-1}), and the total volume of the electrode is calculated on the base of a battery with a capacity of 100 mA h. Table S3† shows the detailed thickness, loading mass, and volumetric capacity in each case.

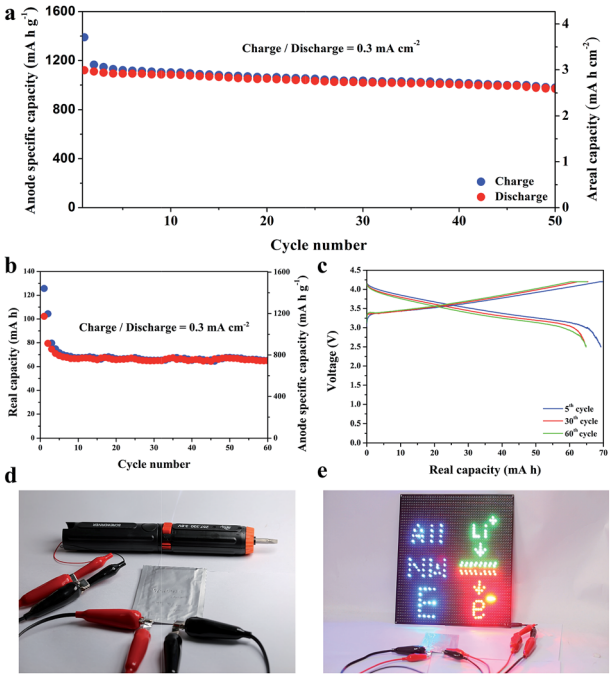

Fig. 7 Full battery composed of a bilayer Ge/Cu nanowire mesh anode and a commercial $Li(Ni_{0.5}Co_{0.3}Mn_{0.2})O_2$ cathode and its applications. (a) Specific capacity and areal capacity of the coin full cell at a current density of 0.3 mA cm^{-2}. (b) Cycling performance of a pouch-type battery at a current density of 0.3 mA cm^{-2} between 2.5 V and 4.2 V. (c) Voltage profile of the pouch-type battery corresponding to (b). (d) A power tool was driven by a pouch-type battery. (e) Pouch-type battery lighted up over 150 different color LED arrays.

calculated by the reversible gravimetric capacity of 330 mA h g^{-1} that was normally exhibited by the anode composed of 94% graphite. The mass of the whole electrode, comprising graphite, non-active materials, and copper foil, was 0.53 g, whereas the approximate volume of the whole electrode was 0.39 cm^{-3}, and the corresponding volumetric capacity was 255 mA h cm^{-3}. For a Ge/Cu mesh electrode with an areal capacity of 3 mA h cm^{-2}, the mass of Ge needed (0.1 g) was calculated by the reversible gravimetric capacity of 1000 mA h g^{-1} normally exhibited by Ge. The mass of the whole electrode was only 0.15 g due to the lighter CuNWs as compared to Cu foil with the same area, and the volumetric capacity was increased to 487 mA h cm^{-3}, which was almost twice that of the graphite/Cu foil electrode. Moreover, other flexible Ge electrodes with CNFs[26,27] as the substrate have extremely low volumetric capacity because the fluffy structure despite CNFs being the lighter substrate can reduce the mass of the whole electrode. Compared to that of the previously reported flexible Ge electrode, the mass of the active material in the Ge/Cu mesh electrode is easily tunable, and the areal capacity over 3 mA h cm^{-2} can be achieved. In addition, owing to the compactly tangled structure of the Ge/Cu nanowire mesh, its volumetric capacity is 10 times as high as that of other flexible Ge electrodes and twice as high as that of graphite; this indicates that the Ge/Cu nanowire mesh provides both high gravimetric and volumetric capacities.

Full cell

Our study demonstrates that the novel bilayer Ge/Cu nanowire mesh structure not only achieves the stable cycling and high rate-capability at a low areal mass loading of Ge (0.5–0.8 mg cm^{-2}), but also maintains the stable cycling performance at a high areal mass loading from around 3 mg cm^{-2} to pair with commercial cathodes. The coin full cells and pouch-type batteries were assembled using $Li(Ni_{0.5}Co_{0.3}Mn_{0.2})O_2$ as a cathode (Fig. S8† shows its half-cell performance) and bilayer Ge/Cu nanowire mesh as an anode. As a result, the areal capacity was still above 2.6 mA h cm^{-2} after 50 cycles at 0.3 mA cm^{-2} (Fig. 7a). Moreover, to accommodate practical applications, a pouch-type battery with the approximate area of 30 cm^2 was prepared and tested between 2.5 and 4.2 V, as shown in Fig. 7b and c, which showed the average discharge working voltage of about 3.4 V. The reversible capacity in the first cycle reached 102 mA h corresponding to the coulombic efficiency 81% at a current density of 0.3 mA cm^{-2}. The discharge capacity retention with regard to the 5th cycle was over 93% after 60 cycles, and this pouch-type battery could drive the power tool and light up over 150 different color LEDs afterwards (Fig. 7d and e).

Conclusion

In conclusion, we proposed a new concept that combines a high theoretical capacity material with the elimination of inactive

materials for maximizing the energy density of lithium-ion batteries. We have designed a bilayer nanowire mesh structure to successfully achieve the abovementioned goal and create a high-performance mesh electrode. Copper nanowires and Ge nanowires spontaneously intertwine at the interface to create good adhesion, and the inactive copper nanowire mesh can be a good substrate to support the fragmented Ge nanowires and provide low-resistance electron channels. In the high areal mass loading test, the bilayer Ge/Cu nanowire mesh electrodes are able to provide a stable areal capacity of approximately 3 mA h cm^{-2}, which can match the commercial electrode in terms of practical applications. Furthermore, the utilization of less amount of copper and active material with higher theoretical capacity significantly reduces the total mass of the electrode; this makes the Ge/Cu nanowire mesh electrode possess better specific capacity and high rate capability than commercial graphite and recent Ge or Si nanostructures based on the total mass of the electrode. In addition, the mass of the active materials of Ge/Cu nanowire mesh can be easily controlled, and its volumetric capacity is 10 times higher than that of other flexible Ge electrodes fabricated with CNFs or graphene. Therefore, the bilayer nanowire mesh electrode provides another train of thought to design the flexible electrodes with both high gravimetric and volumetric energy density for ultralight and ultra-thin lithium-ion batteries.

Conflicts of interest

There are no conflicts to declare.

Acknowledgements

The authors acknowledge the financial support provided by the Ministry of Science and Technology through the grants of NSC 102-2221-E-007-023-MY3, MOST 103-2221-E-007-089-MY3, MOST 103-2622-E-007-025, MOST 102-2633-M-007-002, and MOST 106-2628-E-007-005-MY3.

Notes and references

1 J. Janek and W. G. Zeier, *Nat. Energy*, 2016, **1**, 16141.
2 W. Liu, M.-S. Song, B. Kong and Y. Cui, *Adv. Mater.*, 2017, **29**, 1603436.
3 N. Nitta, F. Wu, J. T. Lee and G. Yushin, *Mater. Today*, 2015, **18**, 252–264.
4 Y. Sun, N. Liu and Y. Cui, *Nat. Energy*, 2016, **1**, 16071.
5 W. Li, X. Sun and Y. Yu, *Small Methods*, 2017, **1**, 1600037.
6 H. Wu, G. Chan, J. W. Choi, I. Ryu, Y. Yao, M. T. McDowell, S. W. Lee, A. Jackson, Y. Yang, L. Hu and Y. Cui, *Nat. Nanotechnol.*, 2012, **7**, 310–315.
7 N. Liu, Z. Lu, J. Zhao, M. T. McDowell, H.-W. Lee, W. Zhao and Y. Cui, *Nat. Nanotechnol.*, 2014, **9**, 187–192.
8 F.-W. Yuan and H.-Y. Tuan, *Chem. Mater.*, 2014, **26**, 2172–2179.
9 D. T. Ngo, H. T. T. Le, C. Kim, J.-Y. Lee, J. G. Fisher, I.-D. Kim and C.-J. Park, *Energy Environ. Sci.*, 2015, **8**, 3577–3588.
10 Y. Zhang, X. Rui, Y. Tang, Y. Liu, J. Wei, S. Chen, W. R. Leow, W. Li, Y. Liu, J. Deng, B. Ma, Q. Yan and X. Chen, *Adv. Energy Mater.*, 2016, **6**, 1502409.
11 W.-C. Chang, K.-W. Tseng and H.-Y. Tuan, *Nano Lett.*, 2017, **17**, 1240–1247.
12 Y. Guo, X. Zeng, Y. Zhang, Z. Dai, H. Fan, Y. Huang, W. Zhang, H. Zhang, J. Lu, F. Huo and Q. Yan, *ACS Appl. Mater. Interfaces*, 2017, **9**, 17172–17177.
13 D. H. Youn, A. Heller and C. B. Mullins, *Chem. Mater.*, 2016, **28**, 1343–1347.
14 J. Ji, Y. Li, W. Peng, G. Zhang, F. Zhang and X. Fan, *Adv. Mater.*, 2015, **27**, 5264–5279.
15 F.-W. Yuan, H.-J. Yang and H.-Y. Tuan, *ACS Nano*, 2012, **6**, 9932–9942.
16 D. T. Ngo, R. S. Kalubarme, H. T. T. Le, J. G. Fisher, C.-N. Park, I.-D. Kim and C.-J. Park, *Adv. Funct. Mater.*, 2014, **24**, 5291–5298.
17 T. Kennedy, E. Mullane, H. Geaney, M. Osiak, C. O'Dwyer and K. M. Ryan, *Nano Lett.*, 2014, **14**, 716–723.
18 K. C. Klavetter, S. M. Wood, Y.-M. Lin, J. L. Snider, N. C. Davy, A. M. Chockla, D. K. Romanovicz, B. A. Korgel, J.-W. Lee, A. Heller and C. B. Mullins, *J. Power Sources*, 2013, **238**, 123–136.
19 J. Liang, X. Li, Z. Hou, T. Zhang, Y. Zhu, X. Yan and Y. Qian, *Chem. Mater.*, 2015, **27**, 4156–4164.
20 X. Li, J. Liang, Z. Hou, Y. Zhu, Y. Wang and Y. Qian, *Chem. Commun.*, 2015, **51**, 3882–3885.
21 M.-H. Park, Y. Cho, K. Kim, J. Kim, M. Liu and J. Cho, *Angew. Chem.*, 2011, **123**, 9821–9824.
22 C. K. Chan, X. F. Zhang and Y. Cui, *Nano Lett.*, 2008, **8**, 307–309.
23 W. Liang, H. Yang, F. Fan, Y. Liu, X. H. Liu, J. Y. Huang, T. Zhu and S. Zhang, *ACS Nano*, 2013, **7**, 3427–3433.
24 R. A. Susantyoko, X. Wang, L. Sun, K. L. Pey, E. Fitzgerald and Q. Zhang, *Carbon*, 2014, **77**, 551–559.
25 J. Wang, J.-Z. Wang, Z.-Q. Sun, X.-W. Gao, C. Zhong, S.-L. Chou and H.-K. Liu, *J. Mater. Chem. A*, 2014, **2**, 4613–4618.
26 W. Li, Z. Yang, J. Cheng, X. Zhong, L. Gu and Y. Yu, *Nanoscale*, 2014, **6**, 4532–4537.
27 W. Li, M. Li, Z. Yang, J. Xu, X. Zhong, J. Wang, L. Zeng, X. Liu, Y. Jiang, X. Wei, L. Gu and Y. Yu, *Small*, 2015, **11**, 2762–2767.
28 C. D. Wang, Y. S. Chui, Y. Li, X. F. Chen and W. J. Zhang, *Appl. Phys. Lett.*, 2013, **103**, 253903.
29 R. Mo, D. Rooney, K. Sun and H. Y. Yang, *Nat. Commun.*, 2017, **8**, 13949.
30 C. J. Peng, L. Wang, Q. W. Li, Y. Y. Li, K. Huo and P. K. Chu, *ChemElectroChem*, 2017, **4**, 1002–1006.
31 X. Lu, J. T. Harris, J. E. Villarreal, A. M. Chockla and B. A. Korgel, *Chem. Mater.*, 2013, **25**, 2172–2177.
32 H.-C. Chu, Y.-C. Chang, Y. Lin, S.-H. Chang, W.-C. Chang, G.-A. Li and H.-Y. Tuan, *ACS Appl. Mater. Interfaces*, 2016, **8**, 13009–13017.
33 A. M. Chockla, T. D. Bogart, C. M. Hessel, K. C. Klavetter, C. B. Mullins and B. A. Korgel, *J. Phys. Chem. C*, 2012, **116**, 18079–18086.

34 D. Y. W. Yu, H. E. Hoster and S. K. Batabyal, *Sci. Rep.*, 2014, **4**, 4562.
35 D.-T. Nguyen, J. Kang, K.-M. Nam, Y. Paik and S.-W. Song, *J. Power Sources*, 2016, **303**, 150–158.
36 D. H. Youn, N. A. Patterson, H. Park, A. Heller and C. B. Mullins, *ACS Appl. Mater. Interfaces*, 2016, **8**, 27788–27794.
37 M. Oh, S. Na, C.-S. Woo, J.-H. Jeong, S.-S. Kim, A. Bachmatiuk, M. H. Rümmeli, S. Hyun and H.-J. Lee, *Adv. Energy Mater.*, 2015, **5**, 1501136.
38 V. Etacheri, O. Haik, Y. Goffer, G. A. Roberts, I. C. Stefan, R. Fasching and D. Aurbach, *Langmuir*, 2012, **28**, 965–976.
39 H. Nakai, T. Kubota, A. Kita and A. Kawashima, *J. Electrochem. Soc.*, 2011, **158**, A798–A801.
40 A. Bordes, K. Eom and T. F. Fuller, *J. Power Sources*, 2014, **257**, 163–169.
41 F. Lindgren, C. Xu, L. Niedzicki, M. Marcinek, T. Gustafsson, F. Björefors, K. Edström and R. Younesi, *ACS Appl. Mater. Interfaces*, 2016, **8**, 15758–15766.
42 K. Xu, *Chem. Rev.*, 2014, **114**, 11503–11618.
43 Y.-M. Lin, K. C. Klavetter, P. R. Abel, N. C. Davy, J. L. Snider, A. Heller and C. B. Mullins, *Chem. Commun.*, 2012, **48**, 7268–7270.
44 A. M. Chockla, K. C. Klavetter, C. B. Mullins and B. A. Korgel, *ACS Appl. Mater. Interfaces*, 2012, **4**, 4658–4664.
45 A. M. Chockla, K. C. Klavetter, C. B. Mullins and B. A. Korgel, *ACS Appl. Mater. Interfaces*, 2012, **4**, 4658–4664.
46 M. H. Park, Y. Cho, K. Kim, J. Kim, M. Liu and J. Cho, *Angew. Chem.*, 2011, **50**, 9647–9650.
47 H. Kim, Y. Son, C. Park, J. Cho and H. C. Choi, *Angew. Chem.*, 2013, **52**, 5997–6001.
48 M.-H. Park, K. Kim, J. Kim and J. Cho, *Adv. Mater.*, 2010, **22**, 415–418.
49 K. H. Seng, M.-H. Park, Z. P. Guo, H. K. Liu and J. Cho, *Angew. Chem., Int. Ed.*, 2012, **51**, 5657–5661.
50 M. I. Bodnarchuk, K. V. Kravchyk, F. Krumeich, S. Wang and M. V. Kovalenko, *ACS Nano*, 2014, **8**, 2360–2368.
51 F.-S. Ke, K. Mishra, L. Jamison, X.-X. Peng, S.-G. Ma, L. Huang, S.-G. Sun and X.-D. Zhou, *Chem, Commun.*, 2014, **50**, 3713–3715.
52 D. J. Xue, S. Xin, Y. Yan, K. C. Jiang, Y. X. Yin, Y. G. Guo and L. J. Wan, *J. Am. Chem. Soc.*, 2012, **134**, 2512–2515.
53 L. P. Tan, Z. Lu, H. T. Tan, J. Zhu, X. Rui, Q. Yan and H. H. Hng, *J. Power Sources*, 2012, **206**, 253–258.
54 C. Yao, J. Wang, H. Bao and Y. Shi, *Mater. Lett.*, 2014, **124**, 73–76.
55 M.-H. Seo, M. Park, K. T. Lee, K. Kim, J. Kim and J. Cho, *Energy Environ. Sci.*, 2011, **4**, 425–428.
56 L. C. Yang, Q. S. Gao, L. Li, Y. Tang and Y. P. Wu, *Electrochem. Commun.*, 2010, **12**, 418–421.
57 Y. Hwa, C.-M. Park, S. Yoon and H.-J. Sohn, *Electrochim. Acta*, 2010, **55**, 3324–3329.
58 A. M. Chockla, K. C. Klavetter, C. B. Mullins and B. A. Korgel, *Chem. Mater.*, 2012, **24**, 3738–3745.
59 C. K. Chan, R. N. Patel, M. J. O'Connell, B. A. Korgel and Y. Cui, *ACS Nano*, 2010, **4**, 1443–1450.
60 N. Liu, H. Wu, M. T. McDowell, Y. Yao, C. Wang and Y. Cui, *Nano Lett.*, 2012, **12**, 3315–3321.
61 A. M. Chockla, J. T. Harris, V. A. Akhavan, T. D. Bogart, V. C. Holmberg, C. Steinhagen, C. B. Mullins, K. J. Stevenson and B. A. Korgel, *J. Am. Chem. Soc.*, 2011, **133**, 20914–20921.
62 T. H. Hwang, Y. M. Lee, B.-S. Kong, J.-S. Seo and J. W. Choi, *Nano Lett.*, 2011, **12**, 802–807.
63 N. Liu, Z. Lu, J. Zhao, M. T. McDowell, H. W. Lee, W. Zhao and Y. Cui, *Nat. Nanotechnol.*, 2014, **9**, 187–192.
64 H. Wu, G. Chan, J. W. Choi, I. Ryu, Y. Yao, M. T. McDowell, S. W. Lee, A. Jackson, Y. Yang, L. Hu and Y. Cui, *Nat. Nanotechnol.*, 2012, **7**, 310–315.
65 C. Wang, H. Wu, Z. Chen, M. T. McDowell, Y. Cui and Z. Bao, *Nat. Chem.*, 2013, **5**, 1042–1048.
66 N. Liu, K. Huo, M. T. McDowell, J. Zhao and Y. Cui, *Sci. Rep.*, 2013, **3**, 1919.
67 H. Wu, G. Yu, L. Pan, N. Liu, M. T. McDowell, Z. Bao and Y. Cui, *Nat. Commun.*, 2013, **4**, 1943.